Research Article

Density functional theory driven phononic thermal conductivity prediction of biphenylene: A comparison with graphene

Harish P. Veeravenkata , Ankit Jain [*]

Mechanical Engineering Department, IIT Bombay, India

ARTICLE INFO

ABSTRACT

The thermal transport properties of biphenylene network (BPN), a novel sp^2-hybridized two-dimensional allotrope of carbon atoms recently realized in experiments [Fan et al., Science, 372 852−856 (2021)], are studied using the density functional theory-driven solution of the Boltzmann transport equation. The thermal transport in BPN is anisotropic and the obtained thermal conductivities are more than an order of magnitude lower than that in graphene, despite similar sp^2-hybridized planar-structure of both allotropes. The lower thermal conductivity in BPN is found to originate from enhanced anharmonicity which in turn is a result of reduced crystal symmetry of BPN.

© 2021 Elsevier Ltd. All rights reserved.

1. Introduction

Since the successful exfoliation of graphene from bulk graphite using scotch tape [1], there has been a huge surge in research activities in graphene fueling the discovery of its exceptional material properties [2−6]. Amongst others, graphene has a high room-temperature carrier mobility of ~ 200, 000 $cm^2V^{-1}s^{-1}$ [4], impressive fracture strength of 130 GPa [7], optical transparency [8], ultrabroad optical absorption spectrum [9], and extremely high thermal conductivity in the range of $3000 − 5000$ W/m-K [10−13]. Despite the high carrier mobility and other remarkable material properties, the pristine graphene is a semi-metal which limits its applications in electronics [14]. There is, therefore, a push for the exploration of other carbon-based two-dimensional materials for applications requiring electronic bandgaps such as photo-catalysis, semiconducting devices, sensors, and thermoelectric energy conversion. Many two-dimensional allotropes of carbon, such as graphyne, Ψ-graphene, penta-graphene, etc, are now known and they differ from graphene in the nature/arrangement of cyclic rings and associated bonding characteristics [15−17].

In all of these applications of two-dimensional materials, the material thermal conductivity plays a crucial role in determining the device performance. Since the ultrahigh thermal conductivity

in graphene is understood to originate from its planar structure [18], the other planar allotropes of carbon are also expected to result in high thermal conductivity. However, a computational thermal transport study reported thermal conductivity in γ-graphyne to be 76 W/m-K which is an order of magnitude lower than that in graphene [19]. The authors suggested that the low thermal conductivity in graphyne is due to the weak bond strength of sp-bonded carbon atoms and lower mass density. In contrast, sp bonds are generally stronger than sp^2 bonds and the small difference in mass density could not explain the two-orders of magnitude reduction in the thermal conductivity of graphyne compared to that in graphene.

Yet another computational study on two other computationally-predicted, sp^2-bonded planar allotropes of carbon, dodecagraphene and tetragraphene, resulted in thermal conductivities to be similar to that in graphyne and 80% lower than that in graphene [20]. The authors attributed the low thermal conductivity of these sp^2-bonded allotropes to superstructure-like modes. These studies suggest that it is not clear *a priori* if other planar allotropes of carbon are going to result in high thermal conductivity similar to that of graphene or reduced thermal conductivity similar to that in graphyne.

Recently, biphenylene network (BPN), a planar fully sp^2-hybridized allotrope of carbon (Fig. 1), is experimentally synthesized [21]. As opposed to hexagonal rings, the carbon atoms in BPN are arranged in square, hexagonal, and octagonal rings. The studies on the thermal transport properties of BPN, either experimental or

* Corresponding author.
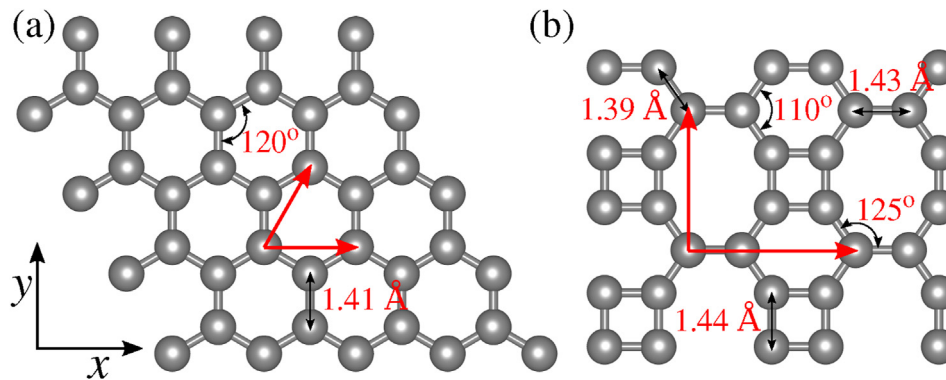*E-mail address:* a_jain@iitb.ac.in (A. Jain).

Fig. 1. The crystal structures of (a) graphene and (b) biphenylene network (BPN). The carbon atoms are arranged in regular hexagons in graphene and in 4-, 6-, and 8-member rings in BPN. The primitive unitcells of graphene and BPN have 2 and 6 atoms respectively. All carbon atoms are sp^2-hybridized in both structures, but while all atoms are equivalent in graphene, they are in two different chemical environments in BPN. (A colour version of this figure can be viewed online.)

computational, are non-existent.

In this work, using ab-initio density functional theory (DFT) driven solution of the Boltzmann Transport Equation (BTE), the thermal transport properties of BPN are investigated and contrasted with graphene. The room temperature thermal conductivity in BPN is obtained as 166 and 254 W/m-K along the orthogonal directions. These values are 16−26 times smaller than the thermal conductivity of graphene, despite planar sp^2 hybridized arrangement of carbon atoms in both BPN and graphene.

2. Methodology

The lattice thermal conductivities are obtained using the iterative solution of the BTE and the required harmonic and anharmonic force constants are obtained from the DFT calculations [22]. As opposed to commonly used relaxation time approximation, the iterative solution of BTE does not treat Normal three-phonon scattering processes as resistive and is found crucial for the correct description of the thermal transport physics in carbon-based materials [18,23,24]. Whilst the full details regarding the calculation of thermal conductivity from the iterative solution of BTE can be found elsewhere [22,25], the thermal conductivity, k_{ph}, is obtained as:

$$k_{ph}^\alpha = \sum_i c_{ph,i} v_\alpha^2 \tau_i^\alpha,$$ (1)

where the summation is over all the phonon modes in the Brillouin zone enumerated by $i \equiv (q, \nu)$, where q and ν are phonon wavevector and mode index, and $c_{ph,i}$, v_α, and τ_i^α represent phonon specific heat, group velocity (α-component), and transport lifetime respectively. The transport lifetimes are obtained by considering phonon-phonon scattering via three-phonon scattering processes and phonon-boundary scattering corresponding to a characteristic length scale, L_{bdry}, of 20 μm, i.e., $1/\tau_{bdry} = L_{bdry}/|\nu|$.

The harmonic force constants are obtained from density functional perturbation theory calculations (DFPT) with an electronic wavevector grid of $8 \times 8 \times 1$ as implemented in the package Quantum Espresso [26,27]. The calculations are initially performed on a phonon wavevector grid of $8 \times 8 \times 1$ and the obtained phonon properties are later interpolated to $48 \times 48 \times 1$ grid for thermal conductivity calculations [28]. The anharmonic force constants are obtained from DFT force-displacement data fitting on 200 thermally populated supercells of size $6 \times 6 \times 1$ (216 atoms) obtained using thermal snapshot technique at a temperature of 300 K [29]. The DFT forces on supercells are evaluated using Gamma-only

sampling of the electronic Brillouin zone. The cubic and quartic interaction cutoffs are set at 5.0 and 2.0 A in the force-displacement data-fitting [30]. The translational invariance constraints are enforced on all extracted force constants. All DFT calculations are performed using planewave energy cutoff of 140 Ry using norm-conserving Von Barth-Car pseudo-potential with local density approximation (LDA) functional as implemented in the package Quantum Espresso [27] and the phonon thermal conductivity calculations are performed using our in-house code. The layer thickness of 3.4 A is assumed for the calculation of phonon heat capacity for both BPN and graphene. All reported thermal conductivities are for isotopically enriched samples, i.e., without considering phonon-isotope scattering. Since both BPN and graphene are relatively stiff materials (as reflected in large phonon group velocities), the anharmonic force constants are obtained only at a temperature of 300 K. The effect of temperature is taken into account in thermal conductivity calculation via phonon-population.

3. Results

The crystal structure of BPN is presented in Fig. 1, along with the structure of graphene. The crystal structure of BPN belongs to the orthorhombic lattice family with a different arrangement of atoms along the x- and y-directions. The primitive unitcell of BPN has six carbon atoms of which four atoms are bonded to other atoms with bond lengths of 1.44, 1.44, and 1.39 A, while the remaining two atoms are bonded to other atoms with bond lengths of 1.39, 1.39, and 1.43 A. The average bond length in BPN is 1.42 A compared to 1.41 A in graphene (all carbon atoms/bonds are identical in graphene). The weak bonding of carbon atoms in BPN is also reflected in its reduced atom density (2.77 A^2/atom compared to 2.58 A^2/atom in graphene) and reduced thermodynamic stability (BPN is 35 mRy/atom higher in energy compared to graphene) as obtained in our DFT calculations. Further, the weak bonding of carbon atoms in BPN results in a larger mean squared thermal displacement of carbon atoms compared to that in graphene. At a temperature of 300 K, we obtain the mean squared thermal displacements of 0.34 (0.31) and 0.31 (0.32) $\times$ 10^{-2} A^2 for the two different kinds of carbon atoms in the x (y) direction in BPN compared to only 0.24 $\times$ 10^{-2} A^2 in graphene.

The phonon dispersion of BPN is presented alongside that of graphene in Figs. 2(a) and 2(b). Overall, the range of vibration frequencies is similar in BPN and graphene. In contrast to graphene, however, BPN has anisotropic dispersion due to its orthorhombic structure. Further, consistent with weak interatomic bonding and higher energy of carbon atoms in BPN, the group velocities of all
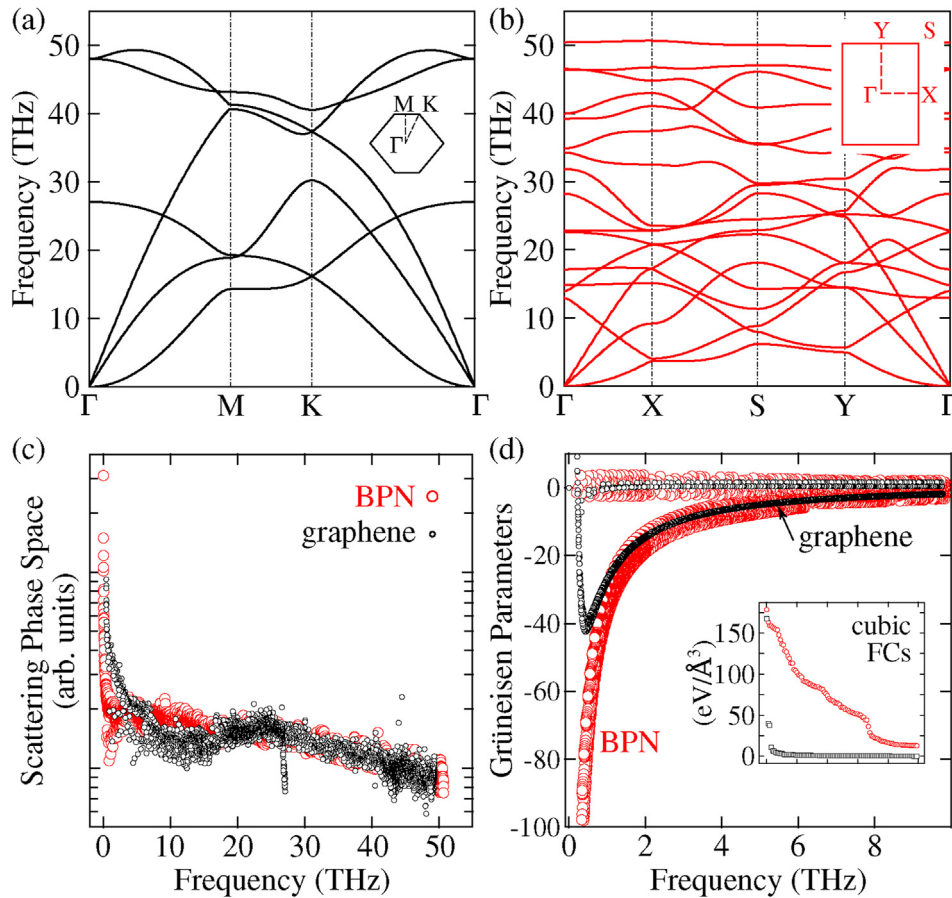
Fig. 2. The phonon dispersion of (a) graphene and (b) BPN. The graphene and BPN have isotropic and anisotropic dispersions with hexagonal and orthorhombic Brillouin zones respectively. The comparison of (c) three phonon scattering phase-space and (d) Grüneisen parameters for graphene and BPN. The strength of 100 largest cubic force constant matrix elements is plotted in the inset to (d). (A colour version of this figure can be viewed online.)

three acoustic phonon branches are severely reduced in BPN compared to that in graphene (18500 and 10670 m/s compared to 20650 and 12340 m/s for longitudinal and transverse acoustic phonons in the long-wavelength limit in the $\Gamma-X$ and $\Gamma-M$ directions in BPN and graphene). In general, a reduction in group velocity results in a decrease in the thermal conductivity of material (according to Eqn. (1)). However, in the case of graphene, the majority of the thermal transport is by flexural phonons having quadratic dispersion and small group velocities. These flexural phonons contribute around 80% to thermal conductivity due to their reduced phonon scattering rates [18]. The possibility and strength of phonon-phonon scattering depend on scattering selection rules and anharmonicity, characterizable using three-phonon scattering phase space and Grüneisen parameters [31,32].

The three-phonon scattering phase-space of BPN is compared with graphene in Fig. 2(c). The scattering phase measures the fraction of total three-phonon processes that are able to satisfy crystal momentum and energy conservation selection rules and is defined here as:

$$P(q,\nu) = \frac{2}{3}\frac{1}{n^2 N}\sum_{q'}\sum_{\nu',\nu''}\delta(\omega(q,\nu)+\omega(q',\nu')-\omega(q+q'-G,\nu''))+ \tag{2}$$

$$\frac{1}{2}\delta(\omega(q,\nu)-\omega(q',\nu')-\omega(q-q'-G,\nu'')), \tag{3}$$

where ω and G represent phonon frequency and reciprocal lattice vector, and n, N are number of phonon branches and wavevectors. The scattering phase-space of BPN is similar to that in graphene for all modes; thus indicating a similar fraction of phonon scattering events are possible in two materials, though the phonon dispersion of BPN is much more complex compared to that of graphene.

Next, the anharmonicity of phonon modes of BPN is characterized using the Grüneisen parameters and is compared with graphene in Fig. 2(d). As can be seen from Fig. 2(d), modes with frequencies larger than 2 THz have similar Grüneisen parameters in BPN and graphene. However, modes with sub-THz frequencies are significantly more anharmonic in BPN compared to that in graphene. The heat capacity weighted average absolute Grüneisen parameter is 6.7 in BPN compared to only 2.7 in graphene at 300 K. To understand the origin of this high anharmonicity of modes in BPN, we compared cubic force constants of BPN with graphene in the inset of Fig. 2(d).

Firstly, we find that due to mirror symmetry, all force constants with an odd number of out-of-plane displacements are zero in BPN, similar to that in graphene. It is worthwhile to note here that this zeroing of cubic force constant elements due to mirror symmetry is argued as the reason for the reduced scattering of flexural phonon modes in graphene [18]. Next, we find that due to the reduced in-plane symmetry of BPN, the number of non-zero cubic force

constant elements are significantly higher in BPN than in graphene. For instance, for the self force-constant matrix, the number of non-zero elements is 14 (out of a total of 27) in BPN compared to only 4 in graphene. Furthermore, the magnitudes of non-zero force constants are much higher in BPN than in graphene. For nearest neighbor interaction in graphene, only 3 elements are non-zero and all three of these non-zero elements have values smaller than 40 eV/A^3. In contrast, for BPN, 22 nearest neighbor cubic matrix elements have values larger than 10 eV/A^3 with two values even larger than 100 eV/A^3.

Moving ahead, we next investigate the thermal conductivity of BPN and plot the results as a function of temperature in Fig. 3. Due to its asymmetric structure, the thermal transport is anisotropic and we report thermal conductivities in both x- and y-directions in Fig. 3(a). The room temperature thermal conductivities are 166 and 254 W/m-K and thermal conductivity decrease with increasing temperature due to enhanced Umklapp phonon-phonon scattering at high temperatures. The lower thermal conductivity in the *x*-direction is understandable from loosely packed atoms with bond-lengths of 1.43, 1.39, 1.44, and 1.39 A for consecutive bonds compared to stronger bonds with bond-lengths of 1.39, 1.44, and 1.39 A in the *y*-direction.

The thermal conductivity of BPN is compared with graphene in Fig. 3(b). Similar to graphene, the phonon-phonon scattering in BPN is dominated by momentum-conserving Normal three-phonon scattering processes. As a result, the correct treatment of phonon-scattering requires an iterative solution of the BTE. The

thermal conductivity obtained from iterative solution is a factor of three higher than that from relaxation time approximation at a temperature of 150 K for BPN compared to a corresponding increase by a factor of seven in graphene. This suggests that even though the scaled three-phonon scattering phase space (and hence the number of scattering processes experienced by phonons) of BPN is similar to that in graphene [see Fig. 2(c)], a much larger fraction of these processes are non-resistive in graphene than that in BPN.

The large fraction of Normal three-phonon scattering processes has an interesting manifestation on the temperature dependence of thermal transport anisotropy. When the Umklapp-scattering processes dominate the phonon scattering, the thermal conductivity decreases with temperature as $1/T$ and the thermal transport anisotropy remains unchanged with temperature. When Normal processes are significant, the temperature dependence of thermal conductivity can deviate from this due to an increase in the fraction of resistive Umklapp processes at higher temperatures. In the case of BPN, this results in a decrease in the thermal transport anisotropy from 1.7 at 150 K to 1.5 at 500 K.

The thermal conductivity of BPN is a factor of 14—29 lower than that of graphene in the considered temperature range. As discussed earlier, this low thermal conductivity of BPN originates from the strong anharmonicity of bonds in BPN compared to that in graphene. Due to this strong anharmonicity, while the contribution of all phonon branches is lower in BPN compared to that in graphene, the reduction is maximum for flexural acoustic phonons which
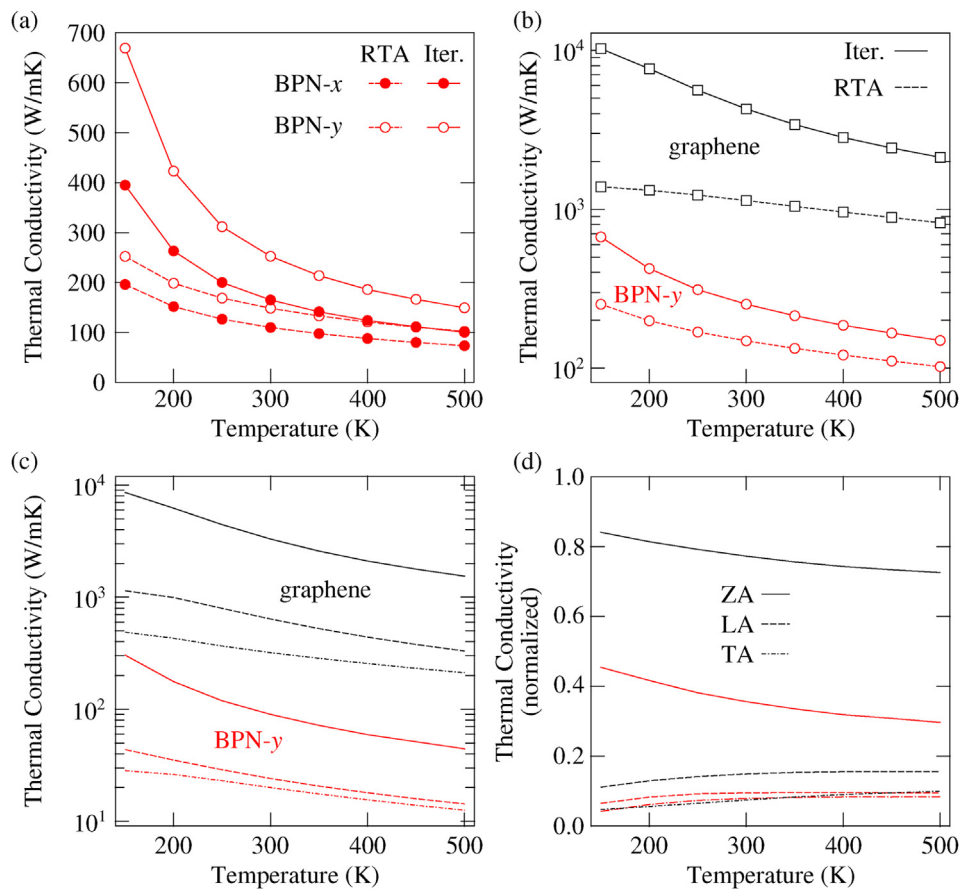

Fig. 3. The temperature-dependent thermal conductivities as obtained from the relaxation time approximation and the iterative solution of the BTE for (a) BPN in the *x*- and *y*-directions and (b) BPN (*y*-direction) and graphene. The temperature-dependent contribution of flexural (ZA), transverse (TA), and longitudinal (LA) acoustic modes towards the thermal conductivity on (c) absolute scale and (d) normalized scale. The values in (d) are normalized by the respective total conductivities of BPN (*y*-direction) and graphene. (A colour version of this figure can be viewed online.)
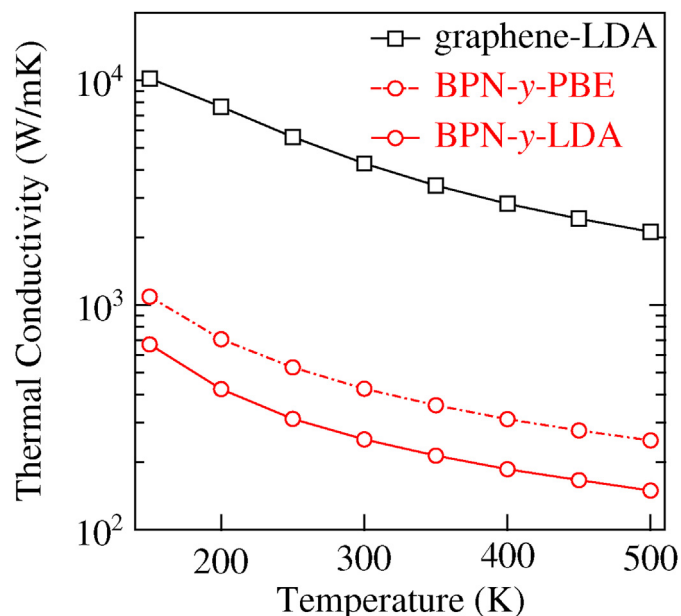
Fig. 4. The role of exchange-correlation functional on the predicted thermal conductivity (from iterative solution) of BPN (y-direction). (A colour version of this figure can be viewed online.)

contribute 3300 W/m-K to thermal conductivity in graphene and only 90 W/m-K in BPN at a temperature of 300 K [see Fig. 3(c)]. The relative contribution of flexural acoustic phonons to the total thermal conductivity is reduced from 77% in graphene to 36% in BPN at room temperature [Fig. 3(d)]. For transverse and longitudinal acoustic phonons, the combined relative contribution reduces from 22% in graphene to 17% in BPN.

Is it worthwhile to note that the results reported in this work are for a freely suspended monolayer of BPN while the experimentally synthesized samples of BPN are supported on a substrate [21]. In the case of graphene, the thermal conductivity reduces from 3000–5000 W/m-K to 600 W/m-K in going from freely-suspended to supported samples [11]. This factor of five reduction in the thermal conductivity of graphene is due to the suppressed contribution of flexural acoustic phonons in supported samples. Since the contribution of these flexural acoustic phonons is only 36% in BPN (compared to 77% in graphene) at room temperature, we expect a comparable reduction in the thermal conductivity of supported samples.

As has been discussed in the literature, the choice of DFT functional results in significant variations in the predicted thermal conductivity of bulk materials due to variations of harmonic and anharmonic interatomic interactions [32]. These variations are representative of prediction uncertainty and to quantify these uncertainties for BPN, we also performed calculations using Perdew-Burke-Ernzerhof (PBE) [33] exchange-correlation functional. For these calculations, we employed a planewave energy cutoff of 80 Ry, and phonons are initially obtained on a wavevector grid of $12 \times 12 \times 1$ using an electronic wavevector grid of size $12 \times 12 \times 1$ from DFPT calculations. Other computational parameters are kept the same as those discussed earlier for LDA functional. The relaxed lattice constant from PBE functional is 4.47 (3.37) A compared to 4.51 (3.76) A from LDA functional in the x (y) direction. The results obtained with PBE functional are reported in Fig. 4. As can be seen from Fig. 4(b), while there is a 40% difference in the predicted thermal conductivities from LDA vs PBE functional, the values are still an order of magnitude times lower than that of graphene at all

temperatures.

4. Summary

In summary, we used density functional theory calculations to investigate the thermal transport properties of biphenylene network (BPN), which is a planar sp^2 hybridized network of carbon atoms, recently realized in experiments. We find that the thermal transport is anisotropic in BPN and the predicted thermal conductivities are an order of magnitude lower than that in graphene. The origin of this reduced thermal conductivity is identified as enhanced bond anharmonicity originating from reduced crystal symmetries in BPN. The effect of anharmonicity is maximally felt by flexural acoustic modes whose contribution reduces from 77% in graphene to 36% in BPN at room temperature.

The raw/processed data required to reproduce these findings is available on a reasonable request via email.

CRediT authorship contribution statement

Harish P. Veeravenkata: Conceptualization, Investigation, Visualization, Writing − review & editing. **Ankit Jain:** Conceptualization, Supervision, Writing − review & editing, Resources, Funding acquisition.

Declaration of competing interest

The authors declare that they have no known competing financial interests or personal relationships that could have appeared to influence the work reported in this paper.

References

[1] K.S. Novoselov, A.K. Geim, S.V. Morozov, D. Jiang, Y. Zhang, S.V. Dubonos, I.V. Grigorieva, A.A. Firsov, J. Sci. 306 (2004) 666. http://www.sciencemag.org/content/306/5696/666.full.pdf.
[2] K.S. Novoselov, E. McCann, S. Morozov, V.I. Fal'ko, M. Katsnelson, U. Zeitler, D. Jiang, F. Schedin, A. Geim, Nat. Phys. 2 (2006) 177.
[3] F. Schedin, A.K. Geim, S.V. Morozov, E. Hill, P. Blake, M. Katsnelson, K.S. Novoselov, Nat. Mater. 6 (2007) 652.
[4] K. Bolotin, K. Sikes, Z. Jiang, M. Klima, G. Fudenberg, J. Hone, P. Kim, H. Stormer, J Solid State Commun 146 (2008) 351.
[5] G. Wang, J. Yang, J. Park, X. Gou, B. Wang, H. Liu, J. Yao, J. Phys. Chem. C 112 (2008) 8192.
[6] A.K. Geim, K.S. Novoselov, In Nanoscience and Technology: a Collection of Reviews from Nature Journals, World Scientific, 2010, pp. 11–19.
[7] C. Lee, X. Wei, J.W. Kysar, J. Hone, science 321 (2008) 385.
[8] R.R. Nair, P. Blake, A.N. Grigorenko, K.S. Novoselov, T.J. Booth, T. Stauber, N.M. Peres, A.K. Geim, Science 320 (2008) 1308.
[9] Z. Zhang, J. Du, D. Zhang, H. Sun, L. Yin, L. Ma, J. Chen, D. Ma, H.-M. Cheng, W. Ren, Nat. Commun. 8 (2017) 1.
[10] W. Cai, A.L. Moore, Y. Zhu, X. Li, S. Chen, L. Shi, R.S. Ruoff, Nano Lett. 10 (2010) 1645.
[11] J.H. Seol, I. Jo, A.L. Moore, L. Lindsay, Z.H. Aitken, M.T. Pettes, X. Li, Z. Yao, R. Huang, D. Broido, N. Mingo, R.S. Ruoff, J. Sci. 328 (2010) 213. http://www.sciencemag.org/content/328/5975/213.full.pdf.
[12] S. Chen, A.L. Moore, W. Cai, J.W. Suk, J. An, C. Mishra, C. Amos, C.W. Magnuson, J. Kang, L. Shi, R.S. Ruoff, J ACS Nano 5 (2011) 321. http://pubs.acs.org/doi/pdf/10.1021/nn102915x.
[13] A.A. Balandin, J Nat Mater 10 (2011) 569.
[14] F. Xia, D.B. Farmer, Y.-m. Lin, P. Avouris, Nano Lett. 10 (2010) 715.
[15] A.N. Enyashin, A.L. Ivanovskii, Phys. Status Solidi 248 (2011) 1879.
[16] S. Zhang, J. Zhou, Q. Wang, X. Chen, Y. Kawazoe, P. Jena, Proc. Natl. Acad. Sci. Unit. States Am. 112 (2015) 2372.
[17] X. Li, Q. Wang, P. Jena, J. Phys. Chem. Lett. 8 (2017) 3234.
[18] L. Lindsay, D.A. Broido, N. Mingo, J Phys Rev B 82 (2010), 115427.
[19] P. Jiang, H. Liu, L. Cheng, D. Fan, J. Zhang, J. Wei, J. Liang, J. Shi, Carbon 113

(2017) 108.

[20] U. Choudhry, S. Yue, B. Liao, J Phys. Rev. B 100 (2019), 165401.

[21] Q. Fan, L. Yan, M.W. Tripp, O. Krejčí, S. Dimosthenous, S.R. Kachel, M. Chen, A.S. Foster, U. Koert, P. Liljeroth, et al., Science 372 (2021) 852.

[22] A.J. McGaughey, A. Jain, H.-Y. Kim, B. Fu, J. Appl. Phys. 125 (2019), 011101.

[23] L. Lindsay, W. Li, J. Carrete, N. Mingo, D.A. Broido, T.L. Reinecke, J Phys Rev B 89 (2014), 155426.

[24] A. Jain, A.J.H. McGaughey, J Sci. Rep 5 (2015), https://doi.org/10.1038/srep08501 10.1038/srep08501.

[25] A. Jain, Phys. Rev. B 102 (2020), 201201.

[26] S. Baroni, S. de Gironcoli, A. Dal Corso, P. Giannozzi, Rev. Mod. Phys. 73 (2001) 515.

[27] P. Giannozzi, S. Baroni, N. Bonini, M. Calandra, R. Car, C. Cavazzoni, D. Ceresoli, G.L. Chiarotti, M. Cococcioni, I. Dabo, A.D. Corso, S. de Gironcoli, S. Fabris, G. Fratesi, R. Gebauer, U. Gerstmann, C. Gougoussis, A. Kokalj, M. Lazzeri, L. Martin-Samos, N. Marzari, F. Mauri, R. Mazzarello, S. Paolini, A. Pasquarello, L. Paulatto, C. Sbraccia, S. Scandolo, G. Sclauzero, A.P. Seitsonen, A. Smogunov, P. Umari, R.M. Wentzcovitch, J Phys-Condens Mat 21 (2009), 395502.

[28] The Change in Predicted Thermal Conductivity at 300 K Is Less than 4% in Increasing the Phonon Wavevector Grid from $48 \times 48 \times 1$ to $64 \times 64 \times 1$.

[29] O. Hellman, P. Steneteg, I.A. Abrikosov, S.I. Simak, Phys. Rev. B 87 (2013), 104111.

[30] The Cubic Cutoff Employed Here Is Same as that Used in Ref. 23 Using the Same Exchange Correlational Functional and Pseudopotential for Graphene. (Note that even though quartic force constants are used in the force-displacement data fitting, the phonon-phonon scattering is considered only up to three-phonon processes).

[31] A. Jain, A.J.H. McGaughey, J Appl Phys 116 (2014), 073503.

[32] A. Jain, A.J. McGaughey, Comput. Mater. Sci. 110 (2015) 115.

[33] J.P. Perdew, K. Burke, M. Ernzerhof, J Phys. Rev. Lett 77 (1996) 3865.